MODELING OF THE LARGE DEFORMATIONS OF AN EXTREMELY FLEXIBLE ROTOR BLADE

Jérôme Sicard*
Graduate Research Assistant,

Jayant Sirohi
Assistant Professor,

Department of Aerospace Engineering and Engineering Mechanics,
University of Texas at Austin,
Austin, TX 78712, USA.

Abstract

This paper describes the analysis of the steady-state flap bending and twist deformation of an extremely flexible rotor blade. An analytical model tailored towards unconventional blades experiencing very large elastic twist angles is derived. In particular, the bifilar effect arising from the foreshortening of the twisted blade is included. The full non-linear coupled equations of motion are solved using a finite element method. Spanwise distribution of flap bending and twist of an 18-inch diameter rotor with flexible blades rotating at 1200 RPM are predicted for various collective pitch angles, and are correlated with experimental measurements. It is shown that the action of the restoring bifilar pitching moments is significant and that omitting its effect leads to a 50% error in the computation of the blade tip pitch angle. The bifilar effect introduces additional kinetic energy and strain energy terms, and it is seen that the kinetic energy terms are predominant over the strain energy terms. Furthermore, it is shown that conventional analyses derived for rotor blades with small angles of elastic twist cannot predict the large deformation of blades with very low torsional frequencies, on the order of 1.5 per rev.

1 INTRODUCTION

Micro aerial vehicles (MAVs) have become increasingly popular over the past decade as they are capable of fulfilling mission requirements that conventional manned vehicles or larger unmanned aerial vehicles cannot.[1] Among the types of MAVs in development, rotary-wing MAVs offer unique strengths related to their ability to take off and land vertically, hover, and fly at very low advance ratios.[2,3] These qualities make them perfectly suited to indoor surveillance or reconnaissance missions. However, several challenges inherent to the complexity of these missions must be addressed, before fully taking advantage of the benefits. Flying in congested terrain increases the likelihood of blade impact with obstacles. Additionally, the size of the rotor limits the range of motion of the vehicle and its ability to access confined spaces.

These observations motivated Sicard and Sirohi to develop a morphing, damage tolerant rotor for microhelicopters. In this concept, the rotor blades are extremely flexible so that they can be rolled and stowed inside the rotor hub, enabling variation of the rotor diameter in flight. The full retractation of the blades is also advantageous for storage and ground transportation of the MAV. Furthermore, survival of the vehicle upon collision of the rotor with an object is permitted by the high compliance of the blade material. In such an event, the rotor blade can experience very large deformation, and still elastically recover its original shape.

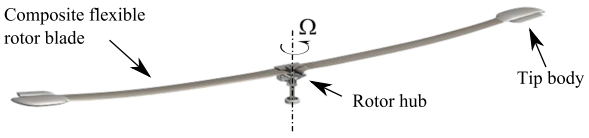

Figure 1: Morphing, damage tolerant flexible rotor concept

A schematic of the flexible rotor concept proposed in this study is shown Fig. 1. The rotor blades are fabricated using composite materials. The choice of the shear modulus of the composite matrix allows for large bending and torsional flexibility (Fig. 2(a)). During flight, stiffening and passive stabilization is achieved by appropriate tailoring of mass and stiffness distributions spanwise. In the flexible blade design shown in Fig. 2(b), this is achieved by securing a mass at the tip of the blade, ahead of the leading-edge of the airfoil.

Because of their relatively low bending and torsional stiffness compared to rigid rotors, extremely

*jerome.sicard@utexas.edu

Presented at the European Rotorcraft 38th Forum, Amsterdam, The Netherlands, September 4-7, 2012.

(a) Flexible rotor at rest, mounted on hover test stand

(b) Flexible blades rotating at 1500 RPM

Figure 2: 18 inch diameter rotor with extremely flexible blades[4]

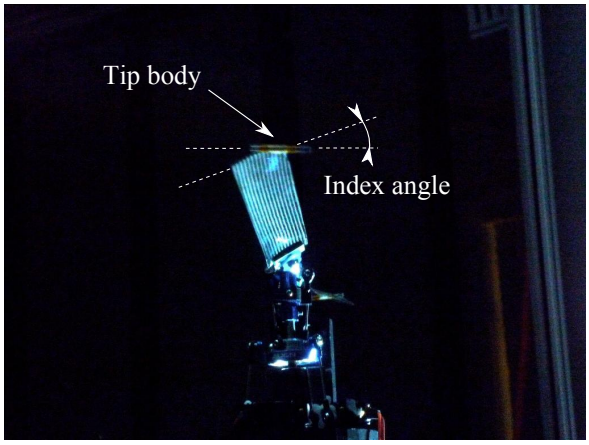

Figure 3: Extremely flexible blade BP (18 inch diameter) rotating at 1500 RPM[5]

flexible blades inherently experience large spanwise bending and twist deformations. In particular, a negative spanwise twist distribution induced by the centrifugal and gravitational forces acting on the tip mass was discovered in a previous study,[4] and can be observed in Fig. 2(b). This large negative twist resulted in poor hover performance. To overcome this issue, blade design parameters such as mass and position of the tip body or blade material properties must be modified. An experimental investigation[5] showed that part of the negative induced twist could be alleviated by changing the orientation of the tip mass, and introducing an index angle between the tip body minor principal axis of inertia and the blade chord. This blade design is shown rotating at 1500 RPM in Fig. 3.

In order to further improve the concept of an extremely flexible rotor, we must be able to predict the steady-state deformations of these unconventional blades and relate the magnitude and variations of the deformations to the design parameters. The objective of this paper is to present an aeromechanics analysis specifically developed to model rotor blades with very low bending and torsional stiffnesses, experiencing large bending and twist deformations.

2 STATE OF THE ART

A recent review on rotor loads prediction by Datta[6] and a review on rotorcraft aeromechanics by Johnson[7] underlined the main publications over the past few decades that have contributed to the development of structural dynamics modeling of rotor blades. The initial form of the partial differential equations of motion for the coupled bending and torsion of twisted nonuniform beams was given by Houbolt and Brooks[8] using a linear analysis. As the significance of non-linear terms in the aeroelasticity of rotary-wings was discovered, non-linear equations of motion for combined flapwise bending, chordwise bending, torsion, and extension of twisted nonuniform rotor blades were derived independently by several authors.[9,10] These theories, accurate to second order, were based on the restriction that non-dimensional bending and torsion deflections were small with respect to unity. Then, in the early 1980s, Hodges[11] and Bauchau[12] addressed larger bending deflections, using a geometrically exact beam theory and a multibody formulation respectively.

More recently, Sicard and Sirohi[13] focused on rotor blades with very low torsional natural frequencies to derive the non-linear aeroelastic equations for combined flapwise bending and twist. The analysis was based on the extended Hamilton's principle. Throughout the derivation, special attention was given

to the terms associated with large twist angles. In particular, the elastic twist angle was considered to be of the same order of magnitude as the control collective pitch angle. In addition, terms related to the bifilar (or trapeze) effect, usually neglected for rotor blades with high torsional stiffness, were retained. This effect induces a radial foreshortening displacement of each cross section of a blade under pure torsion. Also, the analysis included the contribution of the tip body kinetic and potential energies to the total energy of the system. To resolve the non-linear coupled equations of motion, the assumed-modes method was used. The flapwise bending deflections and elastic twist angles obtained by the simulation were compared to experimental measurements obtained using an optical technique called stereoscopic Digital Image Correlation (DIC).[13] Predictions of spanwise blade twist showed good agreement with measurements. In addition, the aeroelastic model matched the slope of the flapwise bending deformation near the root of the blade, but over predicted the tip displacement.

3 PRESENT APPROACH

The present study extends the work of Sicard and Sirohi[13] and focuses on the development of a model capable of predicting accurate steady-state deformations of extremely flexible rotor blades.

First, an alternative technique to find the solution of the equations of motion, based on non-linear Finite Element Method (FEM), is developed.

Then, the results of the analysis are correlated with experimental data. The predicted deformation of a flexible rotor blade are compared to measurements obtained by DIC.[13] Analytical spanwise distribution of flapwise bending deflections and elastic twist angles are validated by comparing them to the experimental measurements for different collective pitch angles.

Finally, the importance of the additional terms retained in the equations of motion of flexible blades, which are neglected in conventional analyses of rigid rotors, is evaluated. The contribution to the total bending deflections and pitch angles of the terms arising from the bifilar effect and the terms retained for arbitrary large elastic twist angles is investigated.

4 ANALYTICAL MODEL

The steady-state equilibrium position of an extremely flexible rotor blade with tip mass can be obtained by retaining the time invariant terms in the extended

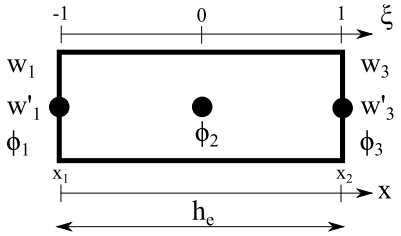

Figure 4: Finite element

Hamilton's principle, written as

$$(1) \quad (\delta T_0 - \delta U - \delta V_g + \delta W_a)_b + (\delta T_0 - \delta V_g)_m = 0$$

where δT_0, δU and δV_g are the variations of time invariant kinetic energy, strain energy and gravitational energy respectively. δW_a is the virtual work done by aerodynamic forces. The subscripts b and m indicate the energies acting on the blade airfoil and the tip mass respectively. The full derivation of the equation of motion is shown in Ref. 13, and the final formulation is given in Appendix A. The terms which differ from conventional analyses that model blades with high torsional rigidity are underlined. Terms underlined by a wavy line are those arising from the bifilar effect. The double underlined terms are retained under the assumption that elastic twist angles are of the same order of magnitude as dimensionless flap deflection. Finally, the terms underlined by a dashline remain for arbitrary non-symmetric blade cross sections. The solution of the equation by FEM is presented hereafter.

Accordingly with the FEM approach, the rotor blade is discretized into a finite number of beam elements. Each beam element has seven degrees of freedom, distributed over three nodes (Fig. 4), which form the elemental generalized coordinates vector:

$$(2) \quad \delta\mathbf{q_i} = \left\{ w_1 \quad w_1' \quad w_2 \quad w_2' \quad \phi_1 \quad \phi_2 \quad \phi_3 \right\}^T$$

Between the elements, there is continuity of displacement and slope for the flap bending deflection, and continuity of displacement for the elastic twist angles. Using appropriate shape functions (Hermite cubic and Lagrange quadratic polynomials for the bending and twist degrees of freedom respectively), we can express the variation of bending $w(x)$ and twist $\phi(x)$ over one element as a function of the generalized coordinates as follows:

$$(3) \quad w(x) = \sum_{i=1}^{2} w_i H_i^0(x) + w_i' H_i^1(x)$$

$$(4) \quad \phi(x) = \sum_{j=1}^{3} \phi_j L_j(x)$$

or in a more compact form:

$$(5) \quad \begin{Bmatrix} w(x) \\ \phi(x) \end{Bmatrix} = \begin{bmatrix} \mathbf{H(x)} \\ \mathbf{L(x)} \end{bmatrix}^T \mathbf{q_i}$$

Upon discretization, the steady-state formulation of the extended Hamilton's principle (Eq.(1)) becomes (6)

$$\sum_{i=1}^{N} \left(\delta T_{0i} - \delta U_i - \delta V_{gi} + \delta W_{ai}\right)_b + \left(\delta T_0 - \delta V_g\right)_m = 0$$

or

$$\sum_{i=1}^{N} \delta E_i + \left(\delta T_0 - \delta V_g\right)_m = 0 \tag{7}$$

where N is the total number of elements and the subscript i indicates that the energy is produced by the i^{th} element. In terms of the generalized coordinates, the variation of energy over one element can be written in the following form:

$$\delta E_i = \delta \mathbf{q_i}^T \left(\mathbf{K q_i} - \mathbf{F}\right)_i \tag{8}$$

The stiffness matrix $\mathbf{K}$ and forcing vector $\mathbf{F}$ are obtained from both the linear and non-linear terms of the equation of motion. The non-linear terms are linearized by Taylor expansion about the equilibrium position found at the previous iteration (Newton-Raphson scheme), as follows:

$$f(\mathbf{q}_{n+1}) = f(\mathbf{q}_n) + \frac{\partial f}{\partial \mathbf{q}}|_{q_n} \left(\mathbf{q}_{n+1} - \mathbf{q}_n\right) \tag{9}$$

The aerodynamic loads acting on each element are derived from a model which relies on quasi-steady aerodynamic assumptions. The lift and aerodynamic pitching moment coefficients are obtained from a lookup table for any given value of angle of attack. In order to evaluate the angle of attack at any radial position as a function of the collective pitch angle, the elastic twist angle and the induced angle, a BEMT model is used.

Summing over all the finite elements and the tip mass, we get

$$\delta \mathbf{q}^T \left(\mathbf{K q} - \mathbf{F}\right) = 0 \tag{10}$$

Note that the energy terms related to the tip mass are treated as boundary conditions, and enter both in the stiffness matrix and the force vector. Because the virtual displacements $\delta \mathbf{q}$ are arbitrary, we finally have

$$\mathbf{K q} = \mathbf{F} \tag{11}$$

This system of equations is solved for the general coordinates q_i's using Gauss elimination, from which we can reconstruct the flap bending and pitch angle as function of span. The flow chart of the algorithm is summarized in Fig. 5.

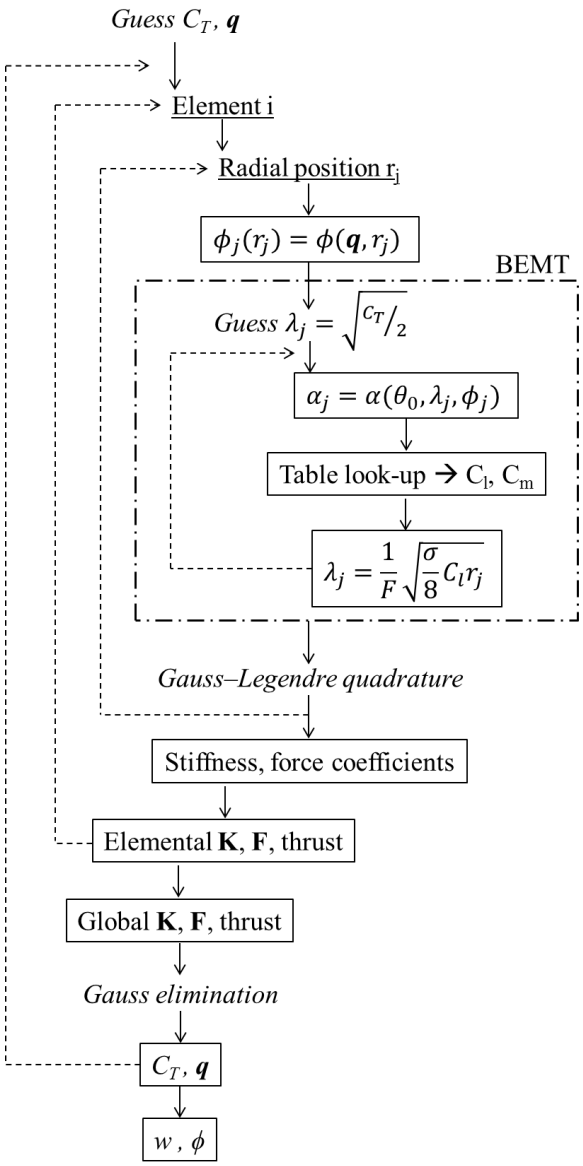

Figure 5: Algorithm flow chart

5 RESULTS AND DISCUSSION

5.1 Correlation of the model with experiment

In order to validate the analysis presented in this paper, we compared experimental measurements of the deformations of an extremely flexible rotor experiencing large torsional deformations to the predicted results.

The parameters of the flexible blade used for the comparison are given in Tables. 1 and 2. To assess of the flexibility of this rotor, we can compare the normalized stiffnesses with that of a conventional rigid

Table 1: Flexible blade parameters

Airfoil parameters						Tip body
Radius R, m	Root cutout, x_0, m	Chord, c, m	Camber, % of chord	Thickness, % of chord	Linear density, m_0, kg/m	Mass, g
0.229	0.059	0.023	7.5	1.39	0.013	2.03

Table 2: Flexible blade normalized stiffnesses

$\frac{EI_\eta}{m_0\Omega^2R^4}$	$\frac{EI_\xi}{m_0\Omega^2R^4}$	$\frac{GJ}{m_0\Omega^2R^4}$
$9.65 \cdot 10^{-2}$	$2.54 \cdot 10^{1}$	$1.00 \cdot 10^{-3}$

rotor blade. For example, the normalized torsional stiffness of a blade of similar cross section, fabricated in carbon fabric / epoxy composite material is equal to 6.64.

Measured and simulated flap bending and torsional deformations experienced by the rotor when spun at 1200 RPM are shown for various collective pitch angles in Fig. 6(a) and 6(b). We can observe that there is very good correlation between the experimental and analytical results. The slope and amplitude of the measured bending deflections are well matched by the analysis. In addition, predictions of spanwise blade twist show very good agreement with experimental data.

As a consequence, the present analytical model is validated and can now be used to investigate the aspects of refined modeling of unconventional flexible blades.

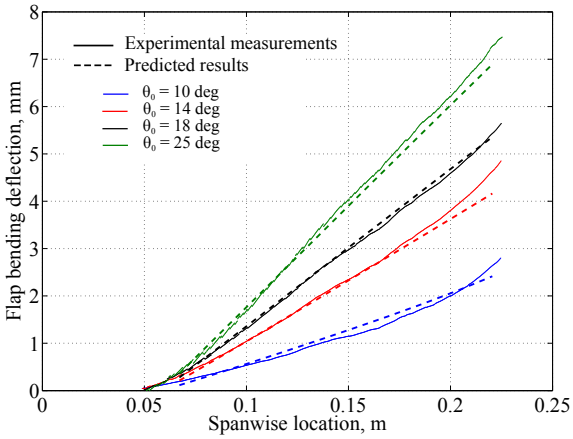

(a) Flap bending deflection

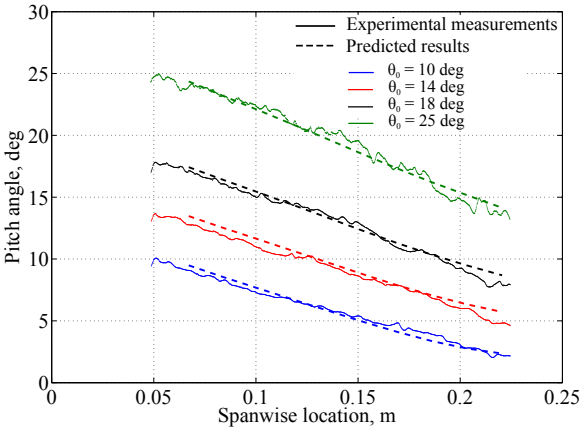

(b) Pitch angle

Figure 6: Predicted and measured deformations of an extremely flexible rotor blade, at 1200 RPM

5.2 IMPORTANCE OF REFINED TORSION MODELING

In this section, the results given by the present analysis focused on rotor blades with very low torsional natural frequencies are compared to those obtained by more conventional analyses developed for stiffer rotors. In particular, the importance of the bifilar effect in the computation of twist deformations is investigated. Secondly, an analysis developed for small elastic twist angles is compared to the present model derived for arbitrary large angles.

5.2.1 Influence of the bifilar effect

The bifilar effect acting on a twisted beam with axial loading is responsible for a torsional moment that tends to restore the beam to its untwisted position. In the case of a rotating blade, the axial loading is the centrifugal force. In order to quantify the magnitude

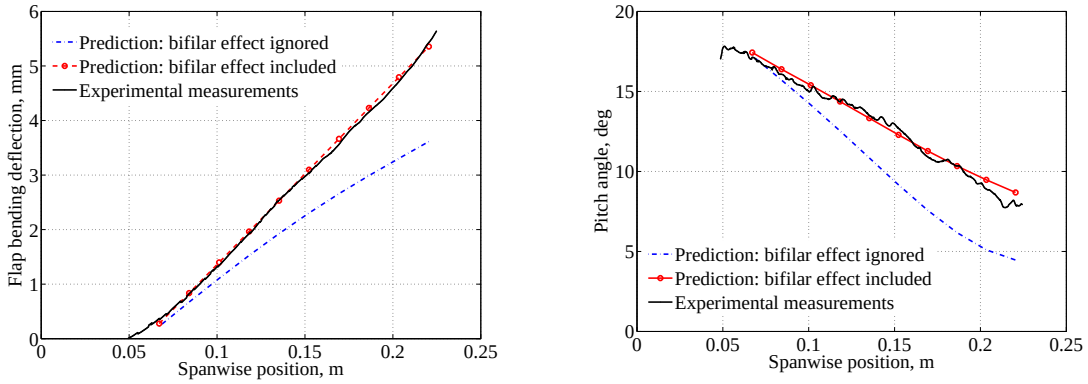

(a) Flap bending deflection

(b) Pitch angle

Figure 7: Influence of the bifilar effect on the deformations of an extremely flexible rotor blade, at 1200 RPM, $\theta_0 = 18$ deg

of the bifilar moment compared to the other pitching moments acting on an extremely flexible rotor blade, each term related to the bifilar effect in the equations of motion was removed, and the corresponding flap bending and twist deformations were simulated. Figures. 7(a) and 7(b) show the contribution of the bifilar term on the deformations of the flexible blade rotating at 1200 RPM. The spanwise distribution of twist shows larger negative (nose-down) pitch angles for the case where the bifilar moment is ignored. As the bifilar moment is neglected, its effect of acting against the negative propeller moment and negative aerodynamic pitching moment disappears, and the resultant twist along the blade is greater. The effect is also seen on the flapwise bending curves: when the bifilar moment is considered, the magnitude of the blade twist is decreased, hence the angle of attack at each section is larger leading to higher lift and greater flapwise bending deflection.

In order to better understand the origin of the bifilar effect, the contribution of each bifilar term in the equation of motion was investigated. Four cases, in which each bifilar term was separately included to the equation of motion, were simulated. The terms included in each case were:

1. kinetic energy bifilar term acting on the tip mass
2. kinetic energy bifilar term acting on the airfoil
3. strain energy bifilar term acting on the airfoil
4. kinetic energy bifilar terms acting on the tip mass and the airfoil

From Fig. 8(a), corresponding to cases 3 and 4, it can be seen that the main contribution to the bifilar moment comes from the kinetic terms. In addition, comparing cases 1 and 2 in Fig. 8(b), we see that the bifilar restoring pitching moment acting on the tip mass is larger than the one acting on the blade airfoil. Finally, it is shown that in order to obtain an accurate prediction of the spanwise twist distribution of a flexible rotor blade, all the bifilar terms must be included.

5.2.2 Influence of the higher order twist terms

In conventional analyses derived for rigid rotor blades, the elastic twist angles are considered to be of the same order of magnitude as the non dimensional bending deflections. In an ordering scheme based on a parameter ϵ, which is the order of the non dimensional flap deflection, we have

$$\frac{w}{R} = O(\epsilon) \tag{12}$$

$$\phi = O(\epsilon) \tag{13}$$

In the present analysis, the twist angles were assumed to be arbitrary large or, in other words, of order 1. This assumption led to additional terms in the equations of motion (twice underlined in Appendix. A). The importance of these terms in the computation of blade deformations of unconventional flexible rotor was investigated by the following approach.

The deformations of the flexible blade with the parameters shown in Table 1 were predicted by a model derived under the conventional small angle of twist assumption. As a result, all the underlined terms in the equation of motion shown in Appendix. A were omitted, and the trigonometric functions were linearized for small angles ϕ. It was found that under these conditions, this model was unable to converge and find an equilibrium position. Mathematically, this

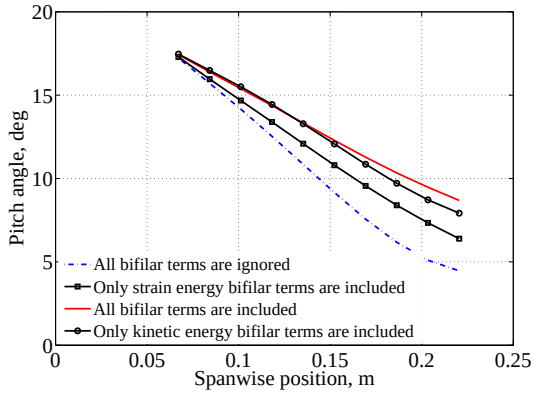

(a) Comparison kinetic energy/strain energy bifilar terms

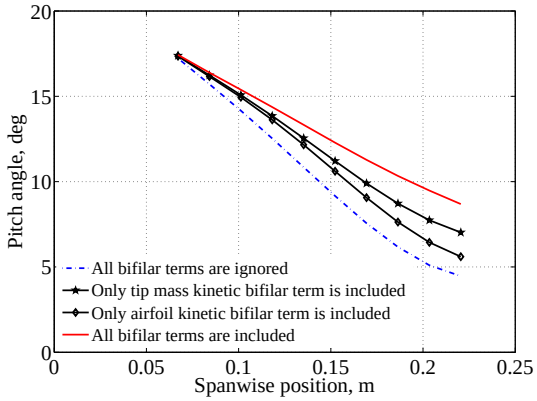

(b) Comparison tip mass/airfoil kinetic energy bifilar terms

Figure 8: Term by term investigation of the influence of the bifilar effect on the twist deformations of an extremely flexible rotor blade, at 1200 RPM, $\theta_0 = 18$ deg

means that the solution was too singular to be approximated by the solver. Physically, this shows that the equation of motion with omitted terms was not representative of the real behavior of an extremely flexible rotor. In fact, it was verified that the model derived for small angles of twist was actually able to converge for normalized stiffnesses of:

$$\frac{EI_\eta}{m_0\Omega^2R^4} = 2.70 \cdot 10^{-1} \tag{14}$$

$$\frac{EI_\xi}{m_0\Omega^2R^4} = 7.12 \cdot 10^{1} \tag{15}$$

$$\frac{GJ}{m_0\Omega^2R^4} = 2.66 \cdot 10^{1} \tag{16}$$

These values correspond to a blade of the same geometry as the blade described in Table. 1, made in Aluminum. Consequently, this investigation shows that the small angle of elastic twist assumption is valid for the prediction of deformation of rigid rotor, but leads to a singular problem for the computation of the deformations of extremely flexible blades.

6 CONCLUSION

The spanwise flap bending and twist distribution of an extremely flexible rotor blade were predicted by an analysis focused towards modeling large torsional deformations. Compared to typical analyses derived for conventional rotors, the present model included additional terms related to the presence of large twist angles. Firstly, the magnitude of the elastic twist was assumed to be of one order of magnitude greater than the non dimensional flap bending deflection. Secondly, the bifilar effect resulting from the foreshortening of the twisted rotor blade was taken into account.

The non-linear coupled equations of motion derived in this study were solved using a finite element approach. Non-linear terms were linearized following a Newton-Raphson scheme, and incorporated to the stiffness matrix and force vector. The predictions of the flap bending and twist deformations of a flexible rotor blade rotating at 1200 RPM were correlated to experimental measurements obtained by stereoscopic DIC. The spanwise variations of the simulated bending deflections and twist angles showed very good agreement with the experimental data.

Then, an extensive investigation on the importance of the bifilar effect in the aeroelastic modeling of blade with low torsional stiffness was conducted. It was found that omitting the bifilar terms led to a 50% error in the computation of the blade tip pitch angle. It was also shown that among the terms arising from the bifilar effect, kinetic energy terms were predominant over the strain energy terms.

Finally, in order to verify the large twist angle assumption made for this analysis, a model derived for small angle and neglecting all higher order twist terms was developed. This model could not converge or find steady-state equilibrium positions for a rotor blade with normalized torsional stiffness of the order of $1 \cdot 10^{-3}$. This confirmed the necessity of considering elastic twist angles as arbitrarily large.

Future plans involve the expansion of the present aeroelastic model to the dynamic analysis of extremely flexible rotors. The objective will be to analytically identify stability boundaries, and correlate the results with experimental observations.

References

[1] Pines, D. J., and Bohorquez, F., "Challenges Facing Future Micro-Air Vehicle Development," *Journal of*

Aircraft, Vol. 43, No. 2, April 2006, pp. 290–305.

[2] Chopra, I., "Hovering Micro Air Vehicles: Challenges and Opportunities," *Proceedings of International Forum on Rotorcraft Multidisciplinary Technology, Seoul, South Korea*, October 2007.

[3] Bohorquez, F., Samuel, P., Sirohi, J., Pines, D., Rudd, L., and Perel, R., "Design, Analysis and Hover Performance of a Rotary Wing Micro Air Vehicle," *Journal of the American Helicopter Society*, Vol. 48, No. 2, April 2003, pp. 80–90.

[4] Sicard, J., and Sirohi, J., "Behavior of an Extremely Flexible Rotor in Hover and Forward Flight," *American Helicopter Society 66th Annual Forum Proceedings, Phoenix, AZ, 11-13 May*, 2010.

[5] Sicard, J., and Sirohi, J., "Twist Control of an Extremely Flexible Rotor Blade for Micro-Aerial Vehicles," *American Helicopter Society International Specialists' Meeting on Unmanned Rotorcraft, Tempe, AZ, 25-27 January*, 2011.

[6] Datta, A., Nixon, M., and Chopra, I., "Review of Rotor Loads Prediction with the Emergence of Rotorcraft CFD," *Journal of the American Helicoter Society*, Vol. 52, No. 4, October 2007, pp. 287–317.

[7] Johnson, W., "Milestones in Rotorcraft Aeromechanics," Ames Research Center 2011-215971, Moffett Field, CA, May 2011.

[8] Houbolt, J. C., and Brooks, G. W., "Differential Equations of Motion for Combined Flapwise Bending, Chordwise Bending, and Torsion of Twisted Nonuniform Rotor Blades," Langley Aeronautical Laboratory, National Advisory Committee for Aeronautics 3905, Langley Field, VA, February 1957.

[9] Hodges, D. H., and Dowell, E. H., "Nonlinear Equations of Motion for the Elastic Bending and Torsion of Twisted Nonuniform Rotor Blades," Ames Research Center and U.S. Army Air Mobility R&D Laboratory NASA TN D-7818, Moffett Field, CA, December 1974.

[10] Kaza, K. R. V., and Kvaternik, R. G., "Nonlinear Aeroelastic Equations for Combined Flapwise Bending, Chordwise Bending, Torsion and Extension of Twisted Nonuniform Rotor Blades in Forward Flight," Langley Research Center, National Aeronautics and Space Administration NASA TM 74059, Hampton, VA, August 1977.

[11] Hodges, D. H., "Geometrically Exact, Intrinsic Theory for Dynamics of Curved and Twisted Anisotropic Beams," *AIAA Journal*, Vol. 41, No. 6, June 2003, pp. 1131–1137.

[12] Bauchau, O. A., and Kang, N. K., "A Multibody Formulation for Helicopter Structural Dynamic Analysis," *Journal of the American Helicopter Society*, Vol. 38, No. 2, April 1993, pp. 3–14.

[13] Sicard, J., and Sirohi, J., "Prediction and Measurement of the Deformations of an Extremely Flexible Rotor using Digital Image Correlation," *American Helicopter Society 68th Annual Forum Proceedings, Fort Worth, TX, 1-3 May*, 2012.

A Steady-state equilibrium equation for an extremely flexible blade with tip mass

$$
\begin{aligned}
(\delta T_0)_b = &\int_{x_0}^{R} \left\{ w' \int_x^R \left(-m_0\Omega^2\chi\right)\, d\chi - m_0\Omega^2 x \left(d_\eta \sin\theta + d_\xi \cos\theta \right) \right\} \delta w' \\
&+ \left\{ - m_0\Omega^2 x w' \left(d_\eta \cos\theta - d_\xi \sin\theta \right) - m_0\Omega^2 \left(k_{m_\xi}^2 - k_{m_\eta}^2 \right) \cos\theta \sin\theta - m_0\Omega^2 k_{m_{\eta\xi}}^2 \left(\cos^2\theta - \sin^2\theta \right) \right\} \delta\phi \\
&+ \left\{ \frac{c^2}{4}\phi' \int_x^R \left(-m_0\Omega^2\chi \right) d\chi \right\} \delta\phi'
\end{aligned}
$$

$$
\begin{aligned}
(\delta U)_b = &\int_{x_0}^{R} \left\{ \left(EI_\xi \sin^2\theta + EI_\eta \cos^2\theta + 2EI_{\eta\xi} \sin\theta\cos\theta \right) w'' - \frac{EB_2}{2}\phi'^2 \sin\theta - \frac{EB_3}{2}\phi'^2 \cos\theta \right. \\
&\left. + EA\frac{c^2}{8}\phi'^2 \left(e_\eta \sin\theta + e_\xi \cos\theta \right) \right\} \delta w'' \\
&+ \left\{ \left(EI_\xi - EI_\eta \right) w''^2 \sin\theta\cos\theta + EI_{\eta\xi} \left(\cos^2\theta - \sin^2\theta \right) w''^2 \right. \\
&\left. - \frac{EB_2}{2} w'' \phi'^2 \cos\theta + \frac{EB_3}{2} w'' \phi'^2 \sin\theta + EA\frac{c^2}{8} w'' \phi'^2 \left(e_\eta \cos\theta - e_\xi \sin\theta \right) \right\} \delta\phi \\
&+ \left\{ \frac{EB_1}{2}\phi'^3 - EB_2 w'' \phi' \sin\theta - EB_3 w'' \phi' \cos\theta + GJ\phi' + EA\frac{c^4}{32}\phi'^3 + EA\frac{c^2}{4} w'' \phi' \left(e_\eta \sin\theta + e_\xi \cos\theta \right) \right. \\
&\left. - EJ\frac{c^2}{4}\phi'^3 \right\} \delta\phi'
\end{aligned}
$$

$$
\begin{aligned}
(\delta V_g)_b = &g \int_{x_0}^{R} m_0 \delta w \\
&- \left\{ m_0 w' \left(d_\eta \sin\theta + d_\xi \cos\theta \right) \right\} \delta w' \\
&+ \left\{ m_0 \left(1 - \frac{w'^2}{2} \right) \left(d_\eta \cos\theta - d_\xi \sin\theta \right) \right\} \delta\phi
\end{aligned}
$$

$$
\begin{aligned}
(\delta W_a)_b = &\int_{x_0}^{R} \left\{ \frac{1}{2} \rho_{air} \left(\Omega x\right)^2 c C_l \right\} \delta w \\
&+ \left\{ \frac{1}{2} \rho_{air} \left(\Omega x\right)^2 c\, x_A C_l + \frac{1}{2} \rho_{air} \left(\Omega x\right)^2 c^2 C_{m_0} \right\} \delta\phi
\end{aligned}
$$

$$
\begin{aligned}
(\delta T_o)_m = &\int_{x_0}^{x_T} \left\{ - m_T\Omega^2 x_T \left(w' \delta w' + \frac{c^2}{4}\phi' \delta\phi' \right) dx \right\} \\
&- m_T\Omega^2 x_T \left\{ \eta_T \sin\theta + \frac{L_2 - L_1}{2} \sin(\theta - \theta_{ind}) \right\} \delta w'_T \\
&- m_T\Omega^2 \left\{ x_T w'_T \left(\eta_T \cos\theta + \frac{L_2 - L_1}{2} \cos(\theta - \theta_{ind}) \right) + \eta_T^2 \cos\theta \sin\theta \right. \\
&\left. + \frac{L_1^3 + L_2^3}{3(L_1 + L_2)} \cos(\theta - \theta_{ind}) \sin(\theta - \theta_{ind}) + \eta_T \frac{L_2 - L_1}{2} \sin(2\theta - \theta_{ind}) \right\} \delta\phi_T
\end{aligned}
$$

$$
\begin{aligned}
(\delta V_g)_m = &m_T g \delta w_T \\
&+ m_T g w'_T \left(\eta_T \sin\theta + \frac{L_2 - L_1}{2} \sin(\theta - \theta_{ind}) \right) \delta w'_T \\
&- m_T g \left(1 - \frac{w'^2_T}{2} \right) \left(\eta_T \cos\theta + \frac{L_2 - L_1}{2} \cos(\theta - \theta_{ind}) \right) \delta\phi_T
\end{aligned}
$$

Note that $\theta(x)$ is the sum of the collective pitch and the elastic twist angle:

$$\theta(x) = \theta_0 + \phi(x)$$